Synthesis of mesostructured metal sulfide films using $[M(H_2O)_n](NO_3)_2$:P85 (M = Cd(II) and Zn(II)) liquid crystalline mesophases

Yurdanur Türker and Ömer Dag*

Received 13th March 2008, Accepted 13th May 2008
First published as an Advance Article on the web 17th June 2008
DOI: 10.1039/b804344b

Transition metal salt–pluronic liquid crystalline (TMS–PLC) mesophases of A–P85, B–P85 and ((1 − *x*)A + *x*B)–P85 (where A is $[Cd(H_2O)_4](NO_3)_2$, B is $[Zn(H_2O)_6](NO_3)_2$ and P85 is a triblock copolymer, $HO(CH_2CH_2O)_{26}(CH_2(CH_3)CHO)_{40}(CH_2CH_2O)_{26}H$) have been used to produce mesostructured metal sulfide films. The TMS–PLC mesophases of A–P85, B–P85 and (A + B)–P85 are well ordered with a salt/P85 mole ratio between 3.0 and 11.0 with a 3D hexagonal structure. The reaction between the mesophases of A–P85, B–P85 and ((1 − *x*)A + *x*B)-P85 and H_2S gas at room temperature produces mesostructured CdS, ZnS and $Cd_{1-x}Zn_xS$ films, respectively. The initial salt concentrations in the TMS–PLC phase determine the final Cd(II) and Zn(II) ions in the $Cd_{1-x}Zn_xS$ crystal structure, where *x* can be controlled between 0.0 and 1.0. Fresh samples of the mesophase reacted under an H_2S atmosphere are continues films that slowly leach out excess P85 producing P85 rich dendrite domains and aggregates of 50 to 100 nm particles of mesostructured CdS, ZnS or $Cd_{1-x}Zn_xS$. However, well homogenized TMS–PLC mesophases produce stable film samples upon H_2S reaction.

1. Introduction

Mesoporous materials[1] were discovered in the early 1990s using the surfactant templating approach. This approach has been expanded to produce many mesostructured insulators,[1–3] semiconductors[4,5] and metals.[6,7] The polymerization of the inorganic/organic precursors (IP/OP) can also be carried in a liquid crystalline mesophase (LCM) to produce mesostructured materials.[3] In the liquid crystalline templating process, the initial mixture (water : surfactant : acid : IP/OP) is usually a liquid that transforms into an LCM and finally to solid mesostructures upon several minutes of aging.[3] This approach has already been employed to produce silica,[3] metal sulfides,[4,5] and metals.[6,7] Kuroda *et al.*[7] have expanded the system using ethanol solutions of a water : salt : surfactant systems that form the LCM with the evaporation of ethanol on an electrode surface to produce mesostructured Pt and Pt–Ru.

Recently, Dag *et al.* have discovered a new LC mesophase that consists of transition metal salt and non-ionic surfactants or pluronics at high metal salt concentrations.[8] The salt–surfactant LC mesophase exist because the metal ions that are dissolved in the media have coordinated water molecules, $M–OH_2$, that induce self-assembly in surfactant molecules to form hexagonal, tetragonal, lamellar and cubic mesophases through hydrogen bonding ($M–OH_2\cdots(OCH_2CH_2)_x$-R) with ethylene oxide units of the surfactant molecules.[5,8] Controlling the quantity and type of the anion (as the counter ion in the metal salt) allows one to control the structure of salt–surfactant LC mesophases.[8c] The mixed salt systems, (A + B)-P85 (where A and B are two different transition metal salts), also form LC mesophases that are important for incorporating more than one type of metal ions at a time into the LC structure and into mesostructured solid materials. Specifically, this allows one to incorporate magnetic or optical components into metal oxides and wide band gap semiconductors, leading to advanced functional materials.

The II–VI semiconductors belong to an important class of materials due to their useful functionality, such as photoluminescence, photonics and photocatalysis.[9,10] The alloy metal sulfides also have the advantage that it is possible to tune the band gaps and, as a result, the optical output of the metal sulfide materials.[11,12]

In this contribution, we have focused on the LC mesophases of the $[Cd(H_2O)_4](NO_3)_2$ and $[Zn(H_2O)_6](NO_3)_2$ salts with P85. As in the individual salt–P85 systems, the mixed salt–P85 systems also form hexagonal mesophases between a salt/P85 mole ratio of 3.0 and 11.0. The TMS–PLC mesophases were reacted under an H_2S gas atmosphere at RT to produce mesostructured $Cd_{1-x}Zn_xS$, where *x* can be controlled between 0.0 and 1.0. $Cd_{1-x}Zn_xS$ and $Cd_{1-x}Mn_xS$ nanocrystallites have been produced in various media,[11,12] however, to the best of our knowledge, this is the first investigation of mesostructured $Cd_{1-x}Zn_xS$ films. The LC mesophase of the mixed salt–P85 systems and mesostructured $Cd_{1-x}Zn_xS$ films have been characterized using XRD, EDS, SEM, TEM, FTIR, micro-Raman, and UV-Vis absorption techniques.

2. Experimental

2.1. Synthesis of CdS, ZnS and $Cd_{1-x}Zn_xS$ in salt:P85 LC media

The $[Zn(H_2O)_6](NO_3)_2$ and $[Cd(H_2O)_4](NO_3)_2$ salts were dissolved in 10 ml ethanol by targeting the total salt surfactant mole ratios of 1.0, 3.0, 5.0, 7.0, 9.0, 11.0, 13.0 and 20.0. To this solution 1.0 g of P85 was added. The resulting solutions were

Laboratory for Advanced Functional Materials, Department of Chemistry and Institute of Materials Science and Nanotechnology – UNAM, Bilkent University, 06800, Ankara, Turkey. E-mail: dag@fen.bilkent.edu.tr; Fax: +90-312-2664068; Tel: +90-312-2903918

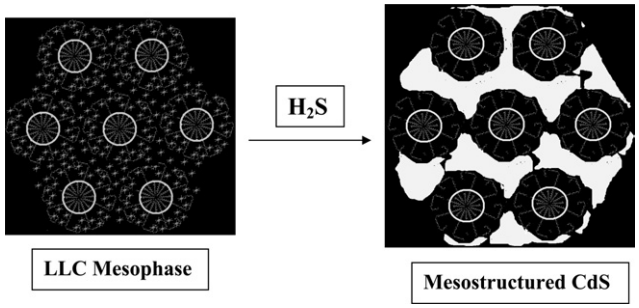

Scheme 1

homogenized by stirring for 3.0 h at RT. The LC thin films of A–P85 and ((1 − *x*)A + *x*B)–P85 were obtained by spin coating 2.0 ml each of the above solutions at 2000 rpm for 30 s and/or dip coating with a speed of 0.4 mm s^{-1} over glass or quartz slides and silicon wafers for XRD, Raman, FTIR and UV-Vis absorption measurements. Then, the LC thin films were exposed to H_2S gas in a gently evacuated reaction chamber (10^{-1}–10 Torr) under 50–450 Torr of H_2S. Most of the experiments were carried out using a solution that contains a 7.0 salt to P85 mole ratio. A typical composition in a 7.0 salt/P85 mole ratio is 0.47 g $[Cd(H_2O)_4](NO_3)_2$: 10 ml C_2H_5OH : 1.00 g P85. The color of the cadmium rich samples changes to yellow in a very short period of time, and they maintain their transparency. However, the zinc rich samples are always colorless and transparent. The LLC mesophase and H_2S reaction are shown schematically in Scheme 1.

2.2. Characterization

X-Ray diffraction (XRD) patterns were recorded on a Rigaku Miniflex Diffractometer using a high power Cu-Kα source operating at 30 kV and 15 mA. The XRD patterns were recorded in small and high angle regions to monitor both the mesophase and nanocrystallites, respectively. FT-IR spectra were recorded using a Bruker Tensor 27 model FTIR spectrometer. A DigiTectTM DLATGS detector was used with a resolution of 4 cm^{-1} and 256 scans in the 400–4000 cm^{-1} range for all samples. The FTIR spectra were recorded in transmittance mode as thin films on a single Si (100) wafer. UV-VIS spectra were recorded using a Varian Cary 5 double beam spectrophotometer with a speed of 150 nm min^{-1} and a resolution of 2 nm over a wavelength range from 800 to 300 nm in transmittance mode. The SEM images were recorded on a ZEISS EVO-40 operating at 15 kV. The samples were prepared on silicon wafers that were attached to aluminium sample holders using conductive carbon adhesive tabs. EDS data and EDS maps were collected using the same SEM using a Bruker AXS XFlash detector 4010. The dark field TEM image was obtained from a thin film sample on a 200 mesh carbon-coated copper grid using Hitachi HD-2000 and JEOL 2100 FX instruments at an accelerating voltage of 200 kV.

3. Results and discussion

3.1. The LC systems of A–P85, B–P85 and (A + B)–P85

Cadmium (A) and zinc (B) nitrate salts can be dissolved in P85 with the help of a solvent, such as ethanol, water or acetone, which enables us to spin or dip coat the salt–P85 LC mesophases. The A–P85 and B–P85 solutions form LC mesophases upon evaporation of the solvent molecules between salt/P85 mole ratios of 3.0 and 11.0. The films obtained using a similar method below and above this range are disordered as investigated by small angle X-ray diffraction (SAXRD) measurements. Fig. 1A

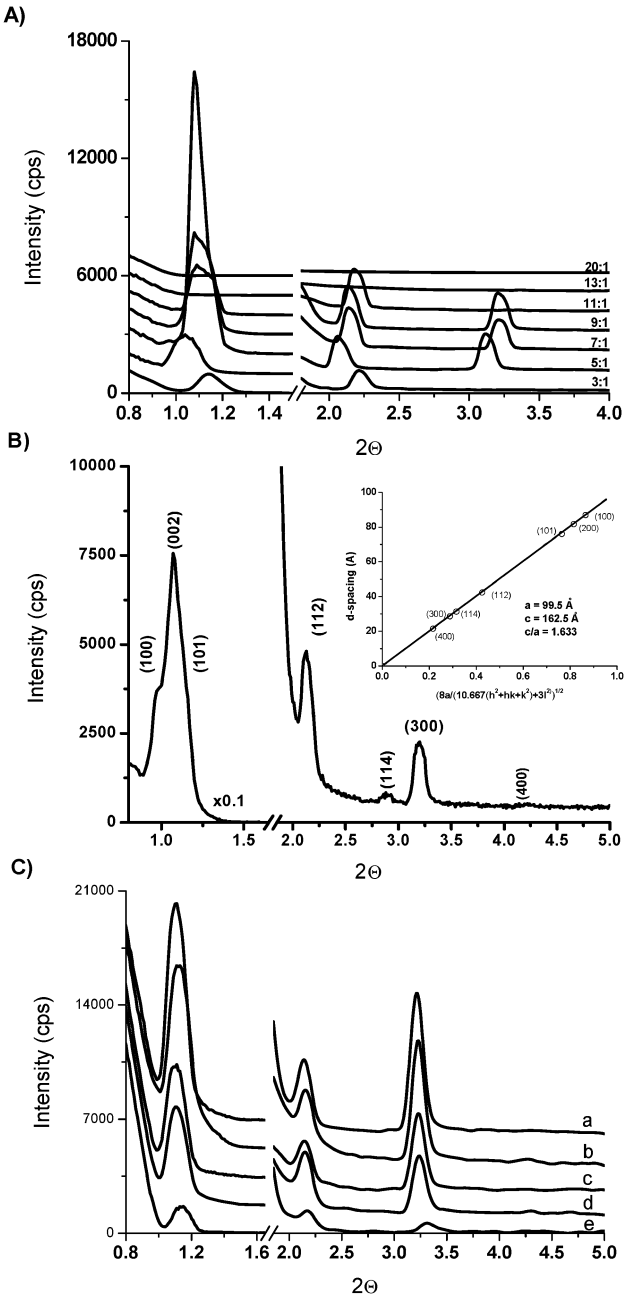

Fig. 1 (A) XRD patterns of the $[Cd(H_2O)_4](NO_3)_2$–P85 with salt/P85 mole ratios as indicated on the diffraction patterns (0.8–1.2° 2θ regions were recorded by blocking the detector with 2 thin Cu plates which reduced the X-ray intensity by 100 times),; (B) XRD pattern of $[Cd(H_2O)_4](NO_3)_2$–P85 with Cd(II)/P85 mole ratio of 7 (prepared using acetone as a solvent); inset in (B) is the plot of *d*-spacing *versus* $8/10.667(h^2 + hk + k^2) + 3l^2)^{1/2}$ obtained from the XRD pattern in (B); (C) XRD patterns of $((1 - x)[Cd(H_2O)_4](NO_3)_2 + x[Zn(H_2O)_6](NO_3)_2$–P85 liquid crystalline mesophases with *x* of a) 1.00, b) 0.75, c) 0.50, d) 0.25, and e) 0.00 with a salt/P85 mole ratio of 7.0.

shows a series of XRD patterns of the thin films with various salt/P85 mole ratios between 3.0 and 20.0. Notice that the salt–P85 samples below 3.0 and above 11.0 mole ratios do not diffract and they are considered disordered, Fig. 1A. However the samples with mole ratios between 3.0 and 11.0 have diffraction lines at small angles that originate from a 3D hexagonal mesophase. The XRD pattern displayed in Fig. 1B shows up to 7 diffraction lines between 0.8 and 5.0°, 2θ range, indexed to (100), (002), (101), (112), (114), (300) and (400) lines, which were observed at 86.8, 81.7, 76, 42.2, 31.3, 28.6 and 21.5 Å d-spacing, respectively, of a $P6_3/mmc$ space group of a 3D hexagonal mesophase. The d *versus* $8/(10.667(h^2 + hk + k^2) + 3l^2)^{1/2}$ (obtained from $1/d^2 = 4/3(h^2 + hk + k^2)/a^2 + l^2/c^2$ relation, where d is d-spacing, a and c are unit cell parameters) plot has a linear correlation and the slope of the plot gives unit cell parameter $a = 99.5$ Å (and $c = 162.5$ Å) with a zero intercept, Fig. 1B (inset). The film sample in Fig. 1B was prepared using a mixture of the $[Cd(H_2O)_4](NO_3)_2$ salt and P85 with a mole ratio of 7.0 in 10.0 ml acetone at RT by the spin coating method at 2000 rpm on a glass substrate. Even though the film samples prepared with 10.0 ml water or ethanol, as described above, had a 3D hexagonal mesophase, they displayed XRD patterns with some diffraction lines missing when compared to the ones prepared using acetone as a solvent, Fig. 1A and B. Therefore the preparation conditions such as type and amount of solvent, duration of stirring, coating rate of the films and thickness of the film strongly influence the order of the film samples. The optimum conditions that we have determined to date include stirring the mixture of $[Cd(H_2O)_4](NO_3)_2$ and P85 in 10.0 ml acetone for an hour at RT, then coating the substrates using ~2.0 ml of the solution at 2000 rpm for 30 s. The film samples prepared under these conditions usually form highly ordered LC mesophases, Fig. 1.

The mixed salt systems, $((1 - x)A + xB)$–P85, also form LC mesophases with the same salt/P85 mole ratios ((A + B)/P85 = 3–11 mole ratio and A = Cd(II), B = Zn(II)). The mesostructures are even more ordered with the same structure in all compositions ($x = 0.0$–1.0) in the mixed salt systems, Fig. 1C. This enables us to homogeneously mix two ions first in the liquid crystalline media then later in the mesostructured $Cd_{1-x}Zn_xS$ lattice (see next section).

3.2. Mesostructured CdS, ZnS and $Cd_{1-x}Zn_xS$ ($x = 0.0$ to 1.0)

The LC film samples were exposed to hydrogen sulfide in an evacuated reaction chamber for between 1 and 15 min. Notice that the mesostructure of the LC phase is stable to vacuum evacuation. Fig. 2 displays the FTIR spectra of a sample prepared using a 7.0 A/P85 mole ratio. The intense signals at 1300 and 1460 cm^{-1} are due to a nitrate ion coordinated to a metal ion.[8d,13] Notice that these two signals completely disappear upon H_2S reaction indicating that the Cd—O_2NO coordination is replaced by Cd–S bonding upon CdS formation. The coordinated water molecules interact with the ethylene oxide (EO) units of P85 through hydrogen bonding, which cause a shift of the C–O stretching of P85 to lower energy. However, upon reaction with H_2S, the C–O stretching frequencies also shift back to free P85 frequencies. Many of the P85 IR modes, observed in the 700–1500 cm^{-1} and 2750–3000 cm^{-1} regions, also respond to the H_2S reaction. The IR spectrum of the fresh sample displays

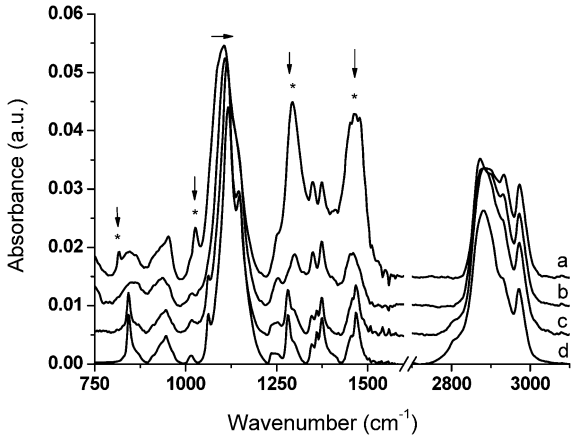

Fig. 2 FTIR spectra of $[Cd(H_2O)_4](NO_3)_2$–P85 a) before and b) 5 min after H_2S reaction, c) sample obtained in b) aged for 5 days, and d) pure P85 (* coordinated nitrate signals, arrows show the behaviour of the peaks in response to H_2S reaction and aging).

broad P85 peaks that become relatively sharp with aging. The comparison of the spectra b) and c) in Fig. 2 clearly shows that some of the surfactant molecules are leaving the mesostructured media, as free P85 upon aging. This was further investigated using SEM and EDS mapping (see text later).

Note also that some of the thin film samples at high salt/P85 mole ratios (7–11 mole ratio) crack upon H_2S reaction. The XRD patterns of the cracked samples display better resolved, small angle diffraction lines, however the crack-free samples display a very broad and weak diffraction at around 1.2° 2θ due to mesostructured metal sulfides, Fig. 3. Fig. 3 also shows a wide angle XRD pattern of a thicker sample that was prepared by reacting salt–P85, with a 20 salt/P85 mole ratio, under H_2S atmosphere. The XRD pattern shows that the mesostructured CdS is made up of zinc blende CdS nanocrystallites. Notice that the cracked samples can display up to 3 diffraction lines at 80.3, 40.1 and 26.8 Å most likely due to (100), (200) and (300) planes of the hexagonal ordering of the CdS nanocrystals, Fig. 3A. Also note that this observation is the first example in the literature in which 3 diffraction lines are observed from mesostructured metal sulfides and/or metals, obtained through LC templating.[4–7] The film samples obtained with a low salt/P85 mole ratio (below 3) and a high salt/P85 mole ratio (above 13) do not diffract before and after the H_2S reaction.

Fig. 4 displays a TEM and two SEM images of a film sample. Both dark field and bright field TEM images show worm-like mesostructures with repeating distance of about 8.0 nm, consistent with the XRD data. The bright regions repeat with 4.0 nm dark domains, corresponding to the P85 regions, throughout the dark field image correspond to the CdS nanoparticles organized into mesostructure. Notice that the high resolution image also shows mesostructure with a crystalline CdS wall and disordered surfactant domains. The SEM images of aged cracked and crack-free samples clearly display film morphology. The crack-free film samples undergo changes over time, producing dendrites in the early stage of aging. Further aging makes the CdS domains aggregate into film islands, Fig. 4B. The as-synthesized samples are uniform and soft. However, the dendrites seem to start forming in various parts of the films and grow into much larger

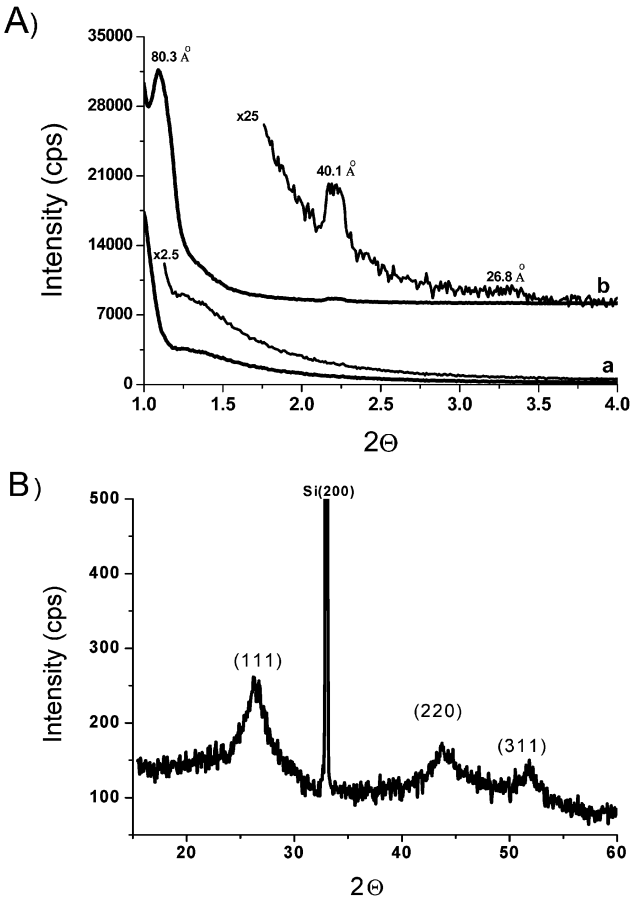

Fig. 3 A) XRD patterns of crack-free (a) and cracked (b) film samples of mesostructured CdS, prepared using a $[Cd(H_2O)_4](NO_3)_2$–P85 LC mesophase with Cd(II)/P85 mole ratio of 7.0; B) high angle XRD pattern of a CdS film sample obtained from a $[Cd(H_2O)_4](NO_3)_2$–P85 mixture with a Cd(II)/P85 mole ratio of 20.

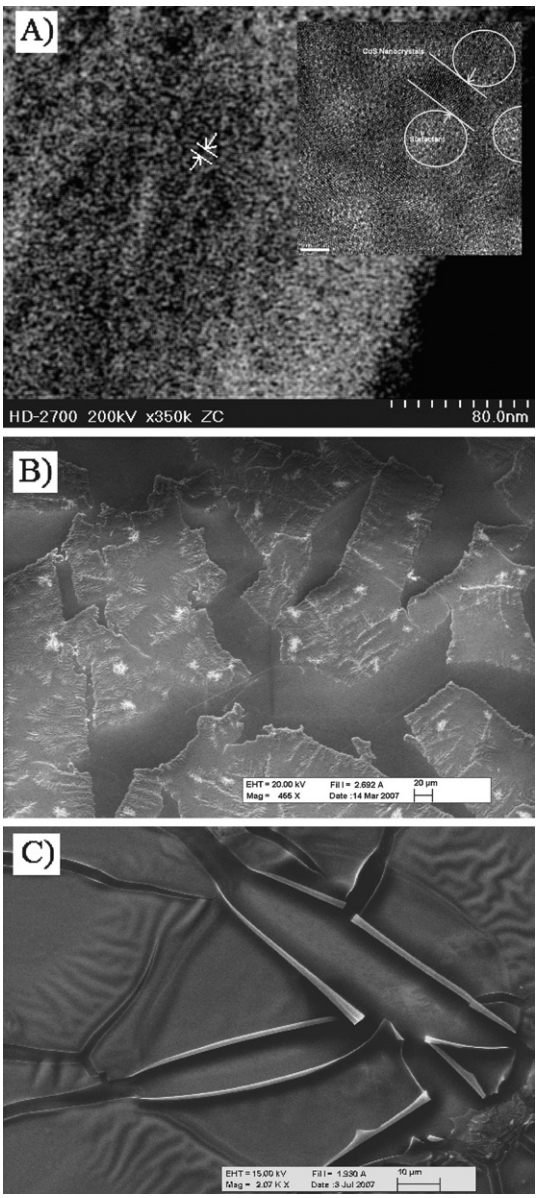

Fig. 4 A) Dark field TEM image of mesostructured CdS films (two lines between the arrows indicate the repeating distance). The inset is a high resolution TEM image. SEM images of B) aged crack-free and C) cracked film samples.

domains in this soft assembly process, Fig. 5. Note also that the number of dendrites decreases with increasing salt concentration in the salt–P85 LC films. Further analysis indicates that the outside regions of the dendrites are made up of aggregates of CdS nanoparticles. Fig. 6A shows a SEM and Cd, S and C EDS maps of a dendrite. The Cd and S EDS maps are identical but the carbon EDS map displays a larger concentration of carbon in the dendrites indicating that some the P85 molecules are leaching out of the structure, Fig. 6A. The SEM image and the EDS maps in Fig. 6B were obtained from the same sample after 10 days of aging and then washing with acetone. Washing with acetone removes most of the free P85 molecules in the regions of dendrites. As shown in Fig. 6B, all the maps, Cd, S, and C, display a similar texture indicating darker regions that are free of Cd and S (no CdS particles) and C (no P85). Identical Cd, S and C EDS maps mean that the CdS nanoparticles are organized by the P85 molecules.

The fresh and aged samples were further analyzed using XRD and UV-Vis absorption techniques. The sharp diffraction lines between 1 and 5 2θ of the as-prepared LC films lose their intensity upon H_2S reaction indicating that the continuous and well ordered mesophase breaks into much smaller domains. However, there is a weak and broad diffraction peak at around 1.2° 2θ that most likely originates from the mesostructured CdS, Fig. 3A. The broad nature of the small angle diffraction is an indication of small mesostructured domains. These observations are consistent with the SEM images and EDS maps that show 100 nm nanoparticles. The nanoparticles aggregate over time to form larger domains. This is also consistent with the observation in the FTIR spectra, which display free P85 signals upon H_2S reaction, correlating the separation of excess P85.

The film samples are thin (as evidenced from the SEM measurement, the thickness is about 150 nm) enough to observe the diffraction lines due to nanocrystalline CdS particles at high angles. However, the diffraction pattern, Fig. 3B, obtained from a thicker sample show that the CdS particles are nanocrystalline and have a zinc blende crystal structure. The particle size (around

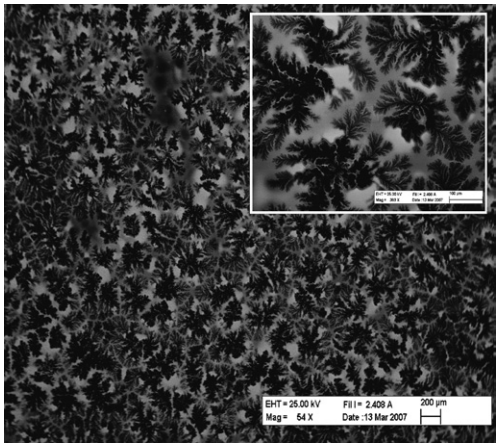

Fig. 5 The SEM image of a large area of dendrites on the mesostructured CdS films, obtained from 7.0 $[Cd(H_2O)_4](NO_3)_2$–P85 mesophase (scale bar is 200 μm). Inset is a magnified image of the same sample (scale bar is 100 μm).

4.3 nm) obtained from the XRD pattern (using Scherrer's equation) is consistent with the particle size observed from the TEM image (see high resolution TEM image in Fig. 4).

The film samples were further analyzed using UV-Vis absorption spectroscopy. Fig. 7A displays a series of UV-Vis absorption spectra of the mesostructured CdS film samples obtained from the 3.0 to 20.0 salt/P85 mole ratios of A–P85 after H_2S reaction. The UV-Vis absorption intensity of the A–P85 samples upon H_2S reaction display a gradual increase above the band edge with increasing metal salt concentration in the reaction media, Fig. 7. The plot of absorbance at 438 nm *versus* salt/P85 mole ratio displays a linear increase in intensity between salt/P85 mole ratios of 3.0 and 11.0. Note also that the absorption edge energy of the samples obtained from the compositions between mole ratios of 3.0 and 11.0 are the same in all samples. Therefore, the particle size must be the same in all samples obtained from the LC mesophases of A–P85, see Table 1.

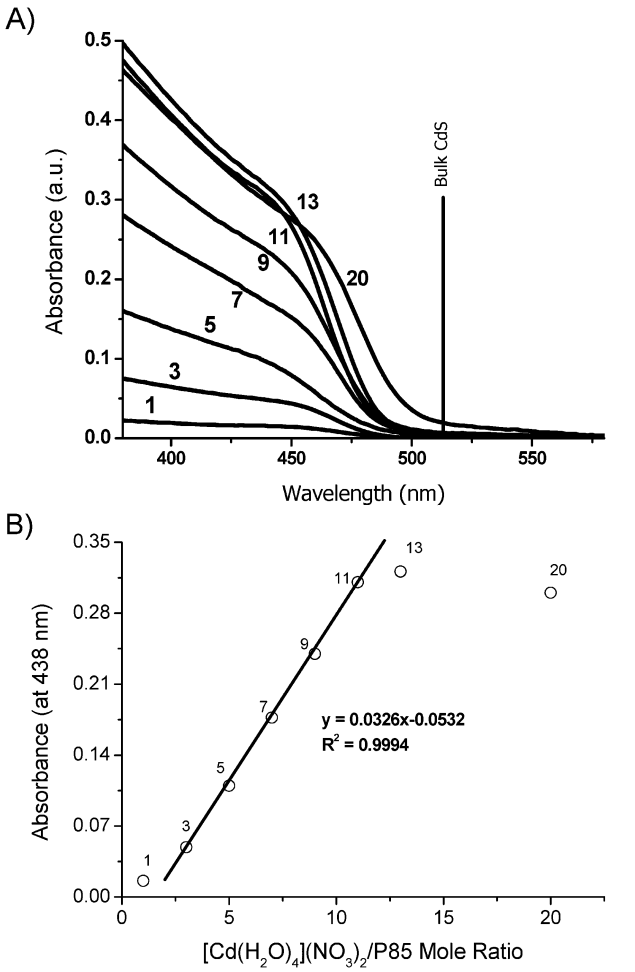

Fig. 7 A) UV-Vis absorption spectra of CdS prepared using $[Cd(H_2O)_4](NO_3)_2$–P85 LC phase with Cd(II)/P85 mole ratios of 1, 3, 5, 7, 9, 11, 13, and 20 (as on the spectra). B) The plot of the intensity at 438 nm with respect to Cd(II)/P85 mole ratio.

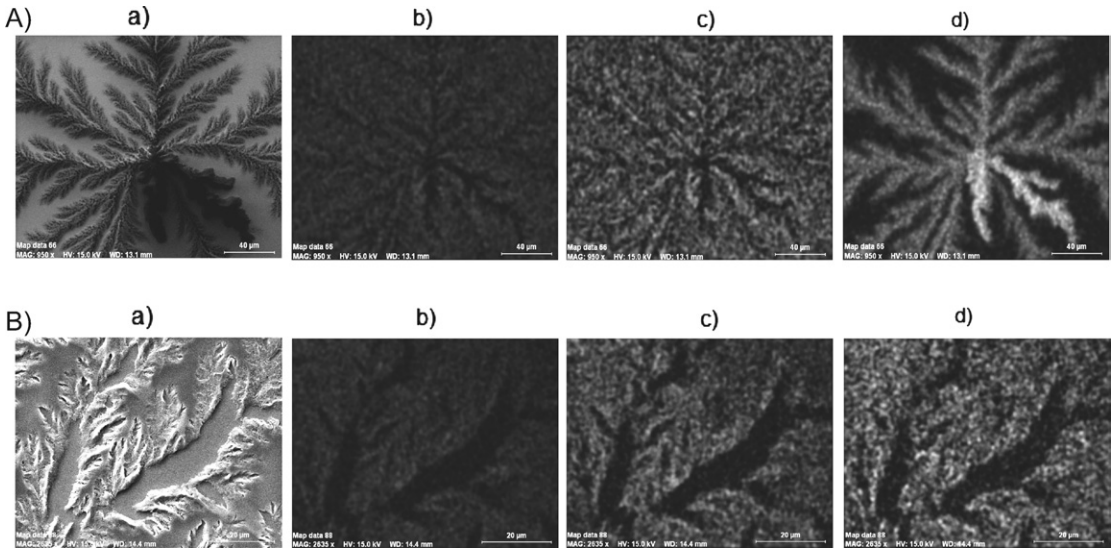

Fig. 6 A) The SEM image (a) and EDS maps ((b) Cd, (c) S, and (d) C) of the as-synthesized mesostructured CdS samples after several hours of aging. B) The SEM image (a) and Cd (b), S (c) and C (d) EDS maps of the film sample in A) that was aged for 10 days and then washed with acetone.

Table 1 The band gap (eV) and particle size (nm) values of CdS at $[Cd(H_2O)_4](NO_3)_2$/P85 mole ratios of 1 : 1 to 20 : 1, calculated from absorption spectra using Sarma's TB model

$[Cd(H_2O)_4](NO_3)_2$/P85 mole ratio	Band gap/eV	Particle size/nm
1	2.60	4.4
3	2.63	4.3
5	2.64	4.1
7	2.61	4.3
9	2.60	4.4
11	2.62	4.3
13	2.60	4.4
20	2.56	5.0

However, at lower and higher concentrations, there is a deviation from linearity in the intensity *versus* salt concentration plot, indicating that the particle size is changing in these compositions. Also notice that the absorption edges of the CdS nanocrystallites with salt/P85 mole ratios below 3.0 and above 11.0, respectively, display a blue and red-shift compared to the samples obtained from the LC mesophases. Large negative deviation at higher salt/P85 ratios is an indication of thinner disordered film samples made up of larger nanocrystallites. Positive deviation observed at lower A/P85 ratios, where there is no order on the mesoscale, most likely originates from the deviation of Beer's law (note that Beer's law deviates positively at low absorbance values) or the formation of thicker film samples. The particle sizes calculated using the absorption band edge and Sarma's[14] Tight Binding (TB) model that was developed for the II–IV semiconductors are tabulated in Table 1. Notice that the particle size at all concentrations is around 4.3 nm, except for the samples obtained from the 20 mole ratio.

As described above the (A + B)–P85 systems also form LC mesophases with salt/P85 mole ratios between 3.0 and 11.0 and form mesostructured $Cd_{1-x}Zn_xS$ thin films upon H_2S reaction. Fig. 8A displays a series of XRD patterns of the $Cd_{1-x}Zn_xS$ samples obtained from a salt/P85 mole ratio of 7.0. The sharp diffraction lines of the LC mesophase disappear upon H_2S reaction. However the weak and broad XRD signal at around 1.2° remains after the H_2S reaction indicating the formation of small mesostructured $Cd_{1-x}Zn_xS$ crystallites. Very similar aging behavior, such as the formation of dendrites, the separation of free P85 and the formation of larger film domains, was observed from the freshly prepared mesostructured $Cd_{1-x}Zn_xS$ samples. Therefore those behaviors are not discussed further in this article.

UV-Vis absorption spectra give insightful information about the $Cd_{1-x}Zn_xS$ samples. Note that band gaps of these two materials are at 2.42 eV in the CdS bulk and 3.68 eV in ZnS.[15] The samples obtained from mixed salt (A + B)–P85 mesophases after the H_2S reaction gradually blue-shift going from the Cd(II) rich samples to Zn(II) samples indicating a homogeneous mixing of Cd(II) and Zn(II) ions in the crystal structure of the $Cd_{1-x}Zn_xS$ nanocrystallites, Fig. 8B. The band-gap energies obtained by fitting the absorption edges of the individual composition to a direct gap relation give band gaps almost linearly proportional to the molar composition of the Zn(II) ion in the crystallites, Fig. 8B. This is consistent with a solid-solution behavior in the $Cd_{1-x}Zn_xS$ nanocrystallites. We have also investigated similar behavior in $Cd_{1-x}Zn_xS$ nanocrystallites prepared in the channels

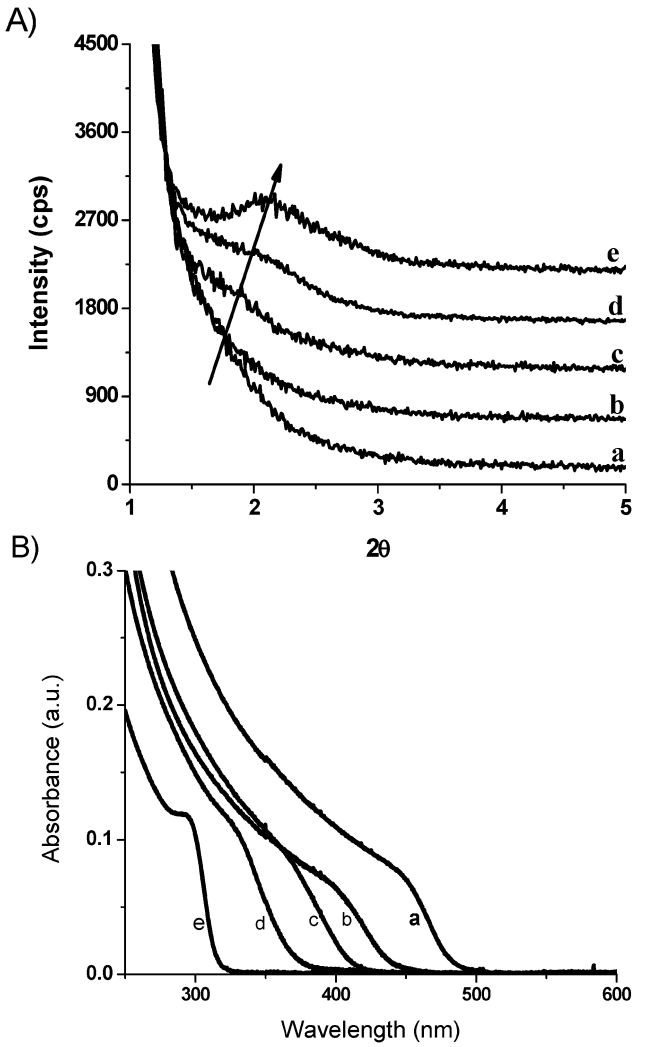

Fig. 8 A) The XRD pattern of the as-synthesized mesostructured $Cd_{1-x}Zn_xS$ using $(1-x)[Cd(H_2O)_4](NO_3)_2 + x[Zn(H_2O)_6](NO_3)_2$–P85 with a salt/P85 mole ratio of 7.0 and B) the UV-Vis absorption spectral changes with x in mesostructured $Cd_{1-x}Zn_xS$; x is a) 0.0, b) 0.3, c) 0.5, d) 0.7 and e) 1.0 in both A) and B).

of mesostructured silica films.[11b] The particle sizes of the nanocrystallites, evaluated using the TB model,[14a] are tabulated in Table 2. The particle size varies between 5.2 and 3.4 nm in the $Cd_{1-x}Zn_xS$ series. Note that the higher solubility of ZnS compared to CdS is the likely origin of the smaller crystallite size at the ZnS end of the series.

The LC ordering in salt–P85 is crucial for the formation of mesostructured metal sulfide films. The homogeneity of the LC

Table 2 The band gap values and particle sizes of the $Cd_{1-x}Zn_xS$ domains of the film samples

Composition	Band gap/eV	Particle size/nm
ZnS	4.00	3.4
$Zn_{0.7}Cd_{0.3}S$	3.51	4.2
$Zn_{0.5}Cd_{0.5}S$	3.16	5.2
$Zn_{0.3}Cd_{0.7}S$	2.91	5.1
CdS	2.62	4.3

mesophases is a very important parameter. Homogenization can be achieved by either stirring the mixture for a long time in a diluted medium or by a few heating and cooling cycles of solvent free samples. The samples prepared by both approaches must be checked using small and high angle XRD measurements. Note that the homogenized samples only diffract at small angles, however the poorly homogenized samples have X-ray diffractions at high angles (between 15 and 40° 2θ) due to crystalline P85 molecules (not shown). Cracked samples were only obtained if the samples were well homogenized before the H_2S reaction in the samples with high salt/P85 mole ratio. The H_2S reaction with the metal ions in the medium is a fast process and produces small metal sulfide nanocrystallites. The film samples undergo phase separation into dendrite domains, free P85 domains and aggregated metal sulfide domains. The origin of this separation is the formation of about 100 nm mesostructured metal sulfide nanoparticles and the presence of excess P85. The salt–P85 mixtures are only liquid crystalline between salt/P85 mole ratios of 3.0 and 11.0. These ratios are 3 to 12 times less when compared to the inorganic/surfactant mole ratios in mesostructured silica and titania. It means that the P85 is 3 to 12 times in excess upon H_2S reaction. This leads to the phase separation and aggregation that yields continuous mesostructured metal sulfide film domains. The free P85 molecules can be washed out of the film samples leaving dendrite empty spaces on the film samples. The most likely origin of the beginning of the dendrite formation seems to be the defects in the salt–P85 LC mesophases. Note that these types of defects are characteristic of lyotropic liquid crystalline mesophases.[16]

We suggest the following formation mechanism for the mesostructured metal sulfides: i) the LC mesophases template the formation of the mesostructured metal sulfide nanoparticles (~100 nm) as evidenced by both XRD patterns and SEM images, ii) since the amount of P85 is much larger than required to form mesostructured metal sulfides, the excess P85 leaches out of the structure and forms dendrites as evidenced using both FTIR and EDS mapping. The most likely origin of the dendrites is the defects where the P85 molecules are disordered and free of metal ions in the LC mesophase as evidenced from the pattern of the dendrites forming over the films (see Fig. 5), iii) the mesostructured metal sulfides aggregate over time around the dendrites to form continuous films (see Fig. 4B), however the stable films do not undergo aggregation and are stable to acetone washing.

4. Conclusion

The transition metal salts ($[Cd(H_2O)_4](NO_3)_2$ and/or $[Zn(H_2O)_6](NO_3)_2$) and pluronic copolymer (P85) form liquid crystalline mesophases that can be used as a template and/or as reaction media to produce mesostructured metal sulfides upon H_2S reaction. The salt ions and pluronic copolymer can be homogeneously mixed either directly or with the help of a solvent, such as water, ethanol or acetone. The acetone or ethanol solution of the salt–P85 mixture can be spin and/or dip coated over various substrates as a thin film. The film samples can keep the LC mesostructures at RT, even under vacuum, upon solvent and free water evaporation. This is very important for the formation of continuous mesostructured films of metal sulfides. The presence of two different salt sources, Cd(II) and Zn(II), does not alter the mesostructure of the film samples.

The (A + B)–P85 LC film samples produce a solid solution of mesostructured $Cd_{1-x}Zn_xS$ films upon H_2S reaction. Note also that the nanoparticles that are organized into mesostructured metal sulfide are smaller in the Zn(II) rich samples. Overall, the film samples are made up of 3.4 to 5.2 nm metal sulfide nanocrystallites that organize into about 100 nm mesostructured metal sulfides. These particles aggregate into nanoporous metal sulfide films over time. The crack-free samples need to be stabilized to produce high quality films that need further studies both before and after H_2S reactions by introducing larger amounts of salt ions into the TMS–PLC media. Furthermore, the method described in this article can also be used to produce other mesostructured alloy metal sulfide and metal selenide thin films.

Acknowledgements

We would like to thank Dr Neil Coombs, Prof. Servet Turan and Hilmi Yurdakul for TEM imaging. For the financial support, ÖD gratefully acknowledges the Scientific and Technical Research Council of Turkey (TÜBİTAK) in the framework of the projects 105T224 and 105M094 and Turkish Academy of Science.

References

1 (*a*) C. T. Kresge, M. E. Leonowicz, W. J. Roth, J. C. Vartuli and J. S. Beck, *Nature*, 1992, **359**, 710; (*b*) T. Yanagisawa, T. Shimizu, K. Kuroda and C. Kato, *Bull. Chem. Soc. Jpn.*, 1990, **63**, 988.
2 (*a*) P. Yang, D. Zhao, D. I. Margolese, B. F. Chmelka and G. D. Stucky, *Nature*, 1998, 396–152; (*b*) D. Zhao, P. Yang, B. F. Chmelka and G. D. Stucky, *Chem. Mater.*, 1998, **10**, 2033.
3 G. S. Attard, J. C. Glyde and C. G. Göltner, *Nature*, 1995, **378**, 366.
4 (*a*) P. V. Braun, P. Osenar and S. I. Stupp, *Nature*, 1996, **380**, 325; (*b*) V. Tohver, P. V. Braun, M. U. Pralle and S. I. Stupp, *Chem. Mater.*, 1997, **9**, 1495; (*c*) 8 X. Jiang, Y. Xie, J. Lu, L. Zhu, W. He and Y. Qian, *Chem. Mater.*, 2001, **13**, 1213; (*d*) P. V. Braun, P. Osenar, M. Twardowski, G. N. Tew and S. I. Stupp, *Adv. Funct. Mater.*, 2005, **15**, 1745.
5 Ö. Dag, S. Alayoğlu, C. Tura and Ö. Çelik, *Chem. Mater.*, 2003, **15**, 2711.
6 (*a*) G. S. Attard, P. N. Barlett, N. R. B. Coleman, J. M. Elliott, J. R. Owen and J. H. Wang, *Science*, 1997, **278**, 838; (*b*) H. Luo, L. Sun, Y. Lu and Y. Yan, *Langmuir*, 2004, **20**, 10218; (*c*) Y. Yamauchi, T. Momma, T. Yokoshima, K. Kuroda and T. Osaka, *J. Mater. Chem.*, 2005, **15**, 1987.
7 (*a*) Y. Yamauchi, T. Ohsuna and K. Kuroda, *Chem. Mater.*, 2007, **19**, 1335; (*b*) Y. Yamauchi, T. Momma, H. Kitoh, T. Osaka and K. Kuroda, *Electrochem. Commun.*, 2005, **7**, 1364.
8 (*a*) Ö. Çelik and Ö. Dag, *Angew. Chem., Int. Ed.*, 2001, **40**, 3800; (*b*) A. F. Demirörs, B. E. Eser and Ö. Dag, *Langmuir*, 2005, **17**, 4156; (*c*) C. Albayrak, G. Gülten and Ö. Dag, *Langmuir*, 2007, **19**, 876; (*d*) Ö. Dag, S. Alayoğlu and İ. Uysal, *J. Phys. Chem. B*, 2004, **108**, 8439.
9 H. Yusuf, W. G. Kim, D. H. Lee, M. Aloshyna, A. G. Brolo and M. G. Moffitt, *Langmuir*, 2007, **23**, 5251.
10 P. V. Kamat and D. Meisel, *Curr. Opin. Colloid Interface Sci.*, 2002, **7**, 282.
11 (*a*) C. Tura, N. Coombs and Ö. Dag, *Chem. Mater.*, 2005, **15**, 573; (*b*) Y. Akdoğan, C. Üzüm, Ö. Dag and N. Coombs, *J. Mater. Chem.*, 2006, **16**, 2048.
12 (*a*) F. J. Brieler, P. Grundmann, M. Fröba, L. M. Chen, P. J. Klar, W. Heimbrodt, H. A. K. von Nidda, T. Kurz and A. Loidle, *J. Am. Chem. Soc.*, 2004, **126**, 797; (*b*) A. V. Kouzema, M. Fröba, L. M. Chen, P. J. Klar and W. Heimbrodt, *Adv. Funct. Mater.*, 2005, **15**, 168.
13 Ö. Dag, O. Samarskaya, C. Tura, A. Günay and Ö. Çelik, *Langmuir*, 2003, **19**, 3671.
14 (*a*) S. Sapra and D. D. Sarma, *Phys. Rev. B*, 2004, **69**, 125304; (*b*) S. Sapra, N. Shanthi and D. D. Sarma, *Phys. Rev. B*, 2002, **66**, 205202.
15 J. Cizeron and M. P. Pileni, *J. Phys. Chem.*, 1995, **99**, 17410.
16 P. J. Collings and M. Hird, *Introduction to Liquid Crystals*, Taylor & Francis Group, London and New York, 1997.